The Gas-Phase Pyrolysis of 2,2-Dinitropropane: Shock-Tube Kinetics

Yi-Xue Zhang and S. H. Bauer*

Department of Chemistry and Chemical Biology, Baker Chemical Laboratory, Cornell University, Ithaca, New York 14853

Received: September 10, 1999; In Final Form: December 7, 1999

The thermal decomposition of 2,2-dinitropropane (DNP) was investigated in a shock tube over the temperature range 970−1200 K, under high dilution in argon at total pressures 4.5−5.5 atm. The decay of DNP and the production of NO_2 were followed spectrophotometrically at 280 and 405 nm, respectively. The derived unimolecular rate constant for dissociation is $k_{uni} = 10^{13.1}$ exp(−23 000/*T*) s^{-1}. The products of pyrolysis were identified and quantitated using FTIR, GC, and GC/MS. The principal products are CO, NO, acetone, $CH_3C{\equiv}H$, $CH_2{=}C{=}CH_2$, CH_3CN, CO_2, CH_3OH, CH_4, H_2O, and CH_2O. The first step in the decomposition appears to be $C-NO_2$ bond fission. However, the temporal profiles of NO_2 during the decomposition are distinctively different from those recorded during the decompositions of CH_3NO_2 or 2-nitropropane, thus pointing to distinctive features in the mechanism. A compilation of 90 elementary steps is proposed. Numerical simulations based on this mechanism reproduce quantitatively the experimentally determined [NO_2] vs time profiles for a range of conditions, as well as the distributions of major products. Sensitivity analysis of the mechanism reveals that only 57 steps are essential for describing the overall pyrolysis under the current experimental conditions. The following intermediates play critical roles in the decomposition: H, OH, NO_2, HCO, and HNO.

Introduction

2,2-Dinitropropane is as strong an explosive as TNT.[1] Its potential use as an explosive and as a possible additive to diesel engine fuel has been reported.[1,2] The *gem*-dinitro functional group characteristic of this compound has been incorporated into many currently used explosives and propellants, TNAZ (1,3,3-trinitroazetidine) for example. In studies of the pyrolysis mechanism of TNAZ,[3−7] a critical question remains unanswered, i.e., whether the reaction is initiated via $C-NO_2$ or $N-NO_2$ bond fission. Experimental data from the pyrolysis of solid TNAZ also suggest that under some conditions the reaction may be initiated by an $N-NO_2$ isomerization.[7] In a series of experimental and theoretical investigations,[8−11] we focused on the decomposition mechanisms of several prototype compounds in order that the thermal decompositions initiated by fissions of different functional groups can be studied separately. The kinetic data from these studies may help identify the initial steps in the pyrolyses of explosives with multiple NO_2 groups. In this report, we describe our investigation of the thermal decomposition of 2,2-dinitropropane (characterized by a *gem*-dinitro group). The initial step of the reaction was identified as $C-NO_2$ bond fission, with an activation energy of 45.7 kcal/mol. A detailed reaction mechanism of 90 elementary steps was proposed to account for the secondary reactions and the formation of the final products. Numerical simulations based on this mechanism quantitatively agree with the experimental results. Contrasts with the pyrolysis of 2-nitropropane are discussed.

Experimental Section

2,2-Dinitropropane was synthesized by the method of Garver, Grakauskas, and Baum.[12] The identity and purity of the sample were confirmed by its NMR and FTIR spectra. The sample was further purified (>95%) by trap-to-trap distillation, with the middle third used for these investigations.

The experimental setup for the shock tube and the diagnostic techniques have been described previously.[10] The shock tube was maintained at 130 °C to prevent condensation of DNP onto the tube walls and connecting lines. The effective residence time under reflected shock conditions was ∼1.3 ms. The initial 2,2-dinitropropane/Ar mixture (∼0.7% mol fraction) was prepared in a ∼6 L Pyrex vessel and allowed to equilibrate at 130 °C prior to use for ∼12 h. The fragmentation reaction was followed spectrophotometrically in real time (18 μs resolution) at two wavelengths: 280 nm for 2,2-dinitropropane and 405 nm for NO_2. The products of the pyrolysis in shock-wave quenched samples were identified and quantitatively determined via GC, FTIR, GC/FTIR, and GC/MS. A total of 61 shock-tube runs were made. Thirty three were monitored spectrophotometrically in the UV, at 280 nm, to follow the decay rate of 2,2-dinitropropane. The temperature and pressure ranges for these experiments were 935−1112 K and 4.5−5.5 atm., respectively. The initial concentrations of 2,2,-dinitropropane in the reflected shock region were $4.5 \times 10^{-7} - 5.2 \times 10^{-7}$ mol/cm^3. To follow the production and decay of NO_2 an additional set of twelve runs was made at 405 nm. The temperatures and pressures for these experiments were 1000−1200 K and 4.6−5.5 atm, maintaining the 2,2-dinitropropane concentration around 5×10^{-7} mol/cm^3. Seven sets of product mixtures were analyzed via FTIR, to determine the levels of CO and NO that were generated. Finally nine runs were carried out for the analysis of products with GC. For these experiments, the temperatures and pressures were 980−1175 K and 4.0−6.0 atm with 2,2-dinitropropane concentrations at $4.5 \times 10^{-7} - 5.5 \times 10^{-7}$ mol/cm^3. Thus, the full temperature range was 935−1200 K, and the pressure range was 4.0−6.0 atm.

10.1021/jp9932057 CCC: $19.00
Published on Web 01/19/2000

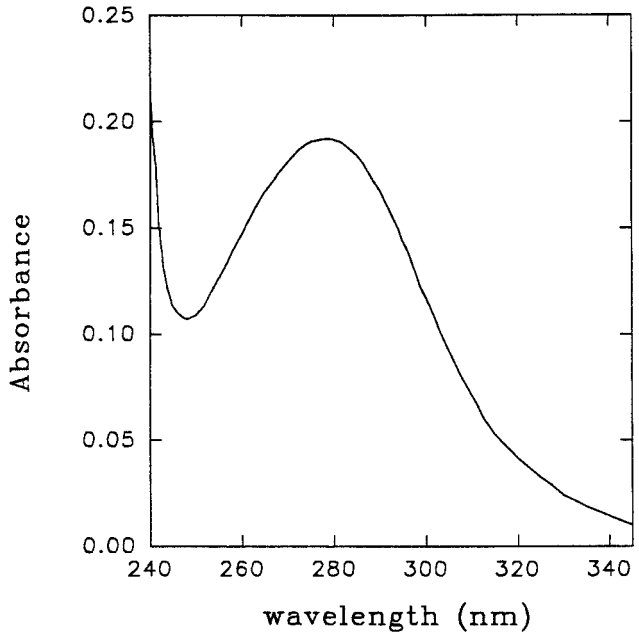

Figure 1. UV spectrum of 2,2-dinitropropane (3.53×10^{-3} M). The solvent is acetonitrile, and the cell length is 1 cm.

The UV spectrum, Figure 1, of DNP (in CH_3CN) was determined with an HP8451A diode array UV−visible spectrophotometer. The extinction coefficient at 277 nm is 55 M^{-1} cm^{-1}. The extinction coefficient of NO_2 can be represented by $\epsilon(M^{-1}\ cm^{-1}) = 179.6 - 0.05475T + 6.33 \times 10^{-6}\ T^2$ at 405 nm, over the temperature range 400−2000 K.[4] The concentrations of CO and NO in the product mixture were determined with a Polaris FTIR spectrometer (Matheson Instruments Inc.). A typical FTIR spectrum of the product mixture is shown in Figure 2. The concentrations of the other reaction products were determined with an HP 18790 chromatograph equipped with a 30 ft × 1/8 in stainless steel Hayesep DB 100/120 packed column; the operational conditions were the same as for the products of pyrolysis of 2-nitropropane.[10] The observed major products are: CO, NO, $(CH_3)_2CO$, $CH_3C{\equiv}H$, $CH_2{=}C{=}CH_2$, CH_3CN, CO_2, CH_3OH, CH_4, CH_2O, and H_2O (not quantitatively determined). Note that the final concentration of NO_2 was too low to be detected in the quenched mixture. There are indications that HNO_3 was also present in the mixture of products, but a quantitative determination of its concentration did not prove feasible.

Results

A unimolecular rate constant for the decay of 2,2-dinitropropane during pyrolysis, in the reflected shock regime, over the temperature range 970−1200 K was derived from first order plots of intensity loss at 280 nm during the early part of the reaction. A typical decay curve is shown in Figure 3. The initial rise in absorbance is due to compression of the sample and the sudden temperature increase in the incident and reflected shock regions. The temperature dependence of the first order rate constant is plotted in Figure 4. The least-squares fitted line can be represented by the following Arrhenius equation:

$$k_{uni} = 10^{13.1\pm0.1} \exp\{(-45.7 \pm 1.7\ \text{kcal/mol})/RT\}\ s^{-1} \quad (1)$$

Since no pressure dependence was observed over the indicated range, we assume that the rate constant is at the high pressure limit.

The temporal profiles of the reactive intermediate NO_2 were monitored at 405 nm. Typical experimental scans are shown in Figures 5 and 6. Because of the presence of two NO_2 groups in the molecule, the peak level of the NO_2 is higher than that recorded during the pyrolysis of 2-nitropropane or nitromethane. The rapid depletion of NO_2 after it reaches its peak value is unusual and merits special consideration. Note that during the pyrolysis of TNAZ (which incorporates three NO_2 groups) large amounts of NO_2 remained in the samples extracted after quenching; in that case there were not sufficient reactive intermediates to consume it.

The measured levels of the major products found in the quenched samples for various temperatures are presented in Figures 7 and 8. CO, NO, and acetone are the most abundant species as was reported by Flournoy.[13] Both $CH_3C{\equiv}CH$ and $CH_2{=}C{=}CH_2$ were identified in the product mixture. Since it is difficult to determine reliably their individual concentrations (due to the overlap of their GC peaks), we plotted their sum vs temperature in Figure 7 (designated C_3H_4). In contrast to the pyrolysis of 2-nitropropane, CH_3CN and CO_2 are major reaction products. Small amounts of CH_4, CH_3OH, and CH_2O were also generated. Note that the major product in the pyrolysis of 2-nitropropane (propylene) was not produced by the dinitro compound.

Discussion

2,2-Dinitropropane has been the subject of many spectroscopic and structural investigations.[14,15] Its thermal decomposition was explored only briefly by Flournoy[13] in 1962. That pyrolysis was carried out in a closed vessel over the temperature range 175−211 °C. Samples taken from the reactor at different times were analyzed with a mass spectrometer. It was found that the initial products were acetone, NO, and NO_2. As the reaction progressed, NO_2 was quickly converted to NO and the final reaction products consisted of H_2O, CO, CO_2, and acetone. The Arrhenius plot from those limited kinetic data was given as

$$k_{uni} = 10^{18.12} \exp\{(-50.5\ \text{kcal/mol})/RT\}\ s^{-1} \quad (2)$$

Note that the preexponential factor is unusually high for a unimolecular process. Flournoy[13] attributed this to a possible chain reaction that may have developed during pyrolysis. However, an unrealistically high *A* factor was also obtained by Flournoy[16] while using the same experimental program for the pyrolysis of dimethylnitramine: $k_{uni} = 10^{20} \exp\{(-53\ \text{kcal/mol})/RT\}\ s^{-1}$. For the latter, a more reliable rate constant was obtained recently by Lin et al.[17] in a shock-tube study, $k_{uni} = 10^{15.9} \exp\{(-43.7\ \text{kcal/mol})/RT\}\ s^{-1}$. In view of the very short temperature range covered in Flournoy's investigation,[13] we question the reliability of his Arrhenius parameters.

The thermochemical parameters of DNP have been considered by several authors.[11,18,19] The predicted $C{-}NO_2$ bond dissociation energy is in acceptable agreement with the activation energy we derived. It is reasonable to conclude that the initial step of the reaction is predominately $C{-}NO_2$ bond fission. Isomerization of $C{-}NO_2$ to C−ONO as a first step in the pyrolysis of nitro compounds has been proposed,[20] but because of the spatial constraints in the *gem*-dinitro group region, we believe that the formation of the cyclic transition state is more difficult for this species than in the decomposition of nitromethane or 2-nitropropane. HONO elimination has been observed in the pyrolysis of nitroethane and 2-nitropropane at low temperatures,[21,22] but at ∼1000 K the contribution from HONO production to the

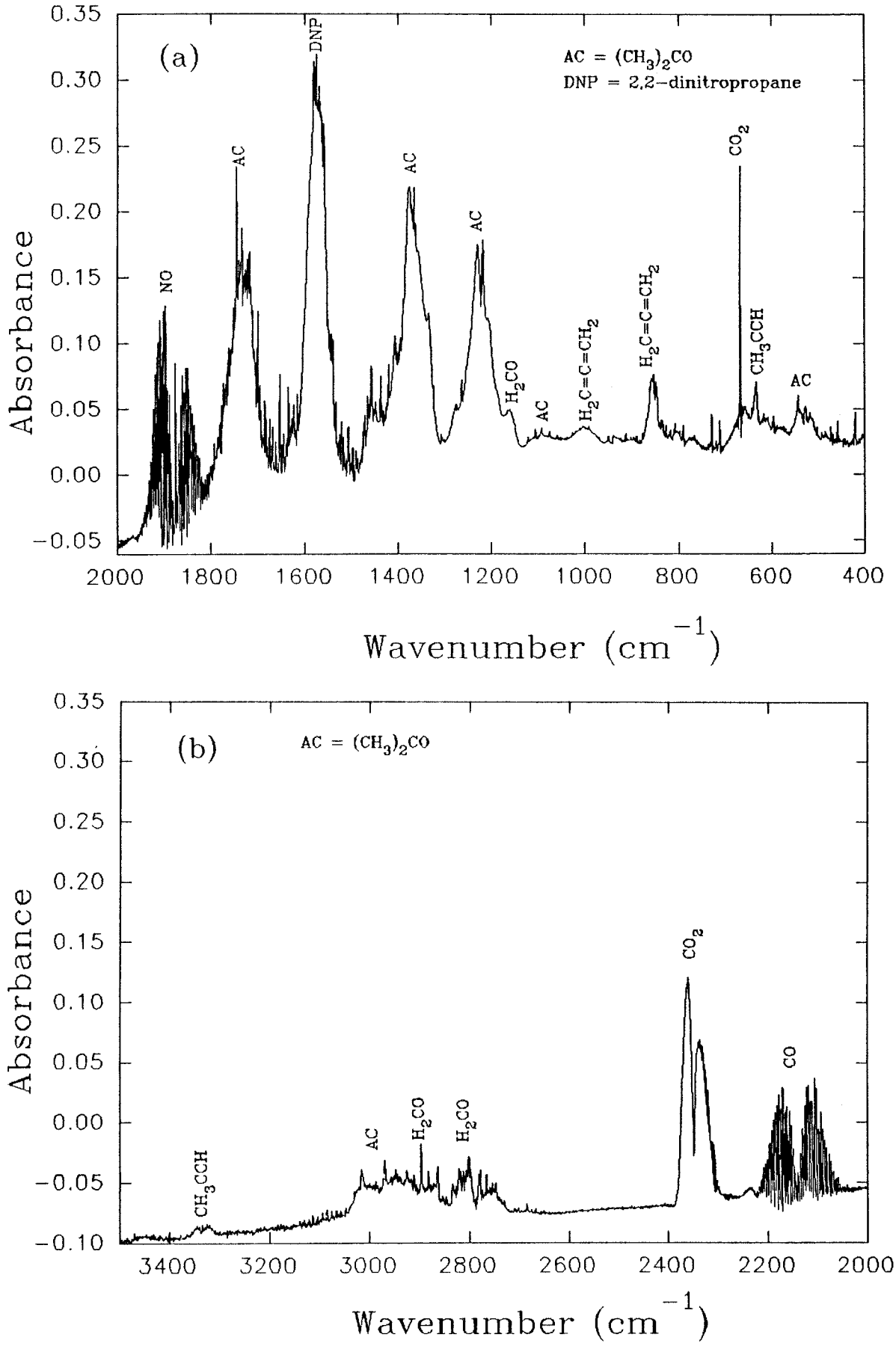

Figure 2. FTIR spectra of shock wave quenched mixture of products, developed during 1.3 ms residence time under reflected shock conditions: $T = 1000$ K, $P = 4.6$ atm Ar; [2,2-dinitropropane $]_o = 4.5 \times 10^{-7}$ mol/cm^3.

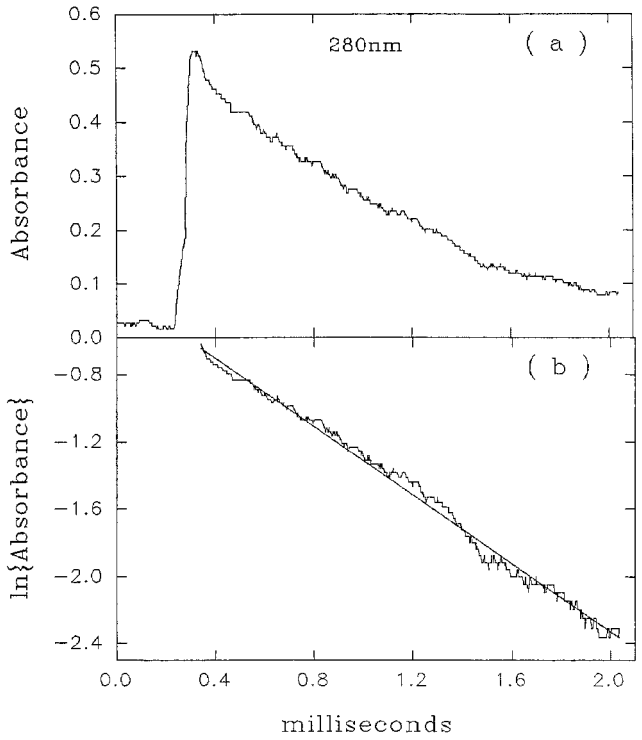

Figure 3. (a) Absorbance vs time (280 nm) during the thermal decomposition 2,2-dinitropropane at 989.6 K. The first slight rise and second major rise in absorbance are due to the very rapid density and temperature increases developed by the incident and reflected shock waves, respectively. Total pressure = 5.12 atm. $[2,2\text{-dinitropropane}]_o = 4.92 \times 10^{-7}$ mol/cm^3. (b) The logarithm of the absorbance vs time curve in (a).

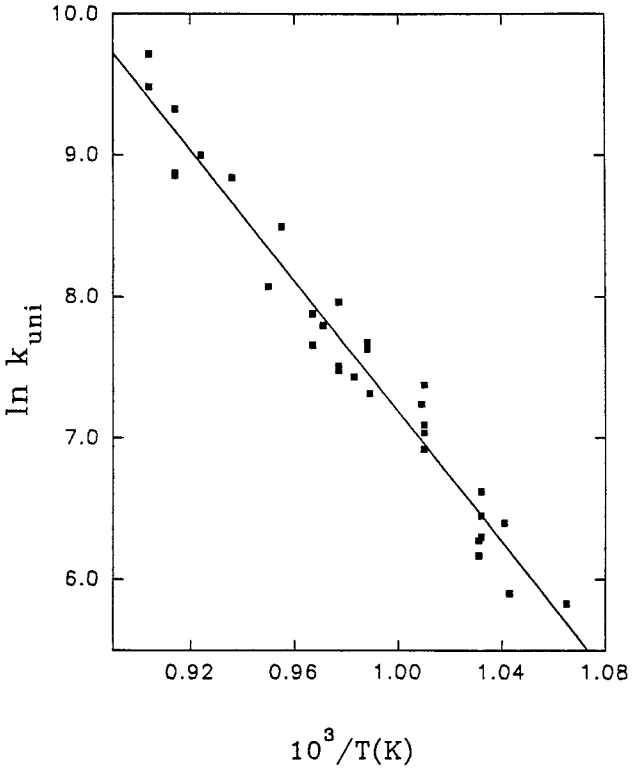

Figure 4. Arrhenius plot for the derived rate constants for 2,2-dinitropropane. Total pressures at reflected shock condition are 4.5−5.5 atm. $[2,2\text{-Dinitropropane}]_o$ is $4.5 \times 10^{-7} - 5.2 \times 10^{-7}$ mol/cm^3. Symbols are experimental values and the solid line is the least-squares fit of the data.

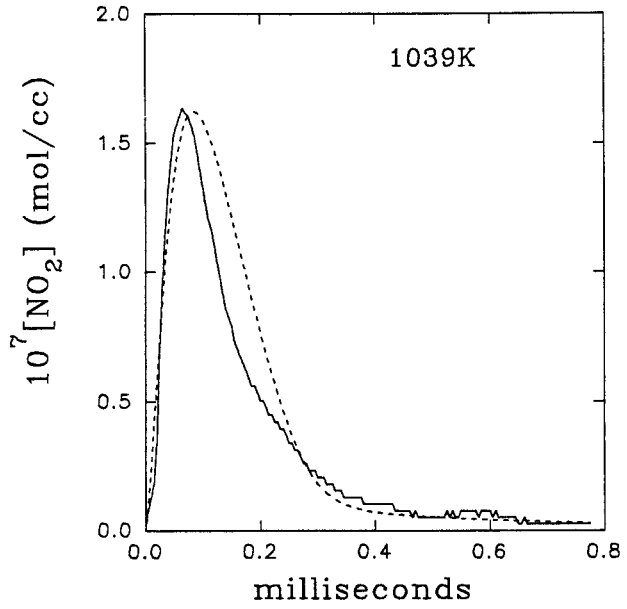

Figure 5. Solid line: Reduced experimentally recorded $[NO_2]$ vs time for DNP. Conditions: $T = 1039$ K, $P = 5.3$ atm, $[2,2\text{-dinitropropane}]_o = 5.1 \times 10^{-7}$ mol/cm^3. The dashed line is the computed $[NO_2]$ vs time curve, per the mechanism in Table 1.

overall decomposition of the above two compounds is negligible. We anticipate a similar situation holds for the pyrolysis of 2,2-dinitropropane.

Several quantum chemical calculations have been made to determine the bond dissociation energies of the $>N-NO_2$ and $(O_2N)(>C)-NO_2$ in order to determine the pyrolysis mechanism of TNAZ.[11,23,24] An assessment can now be made based on experimental data from the studies of the prototype species [dimethylnitramine $(CH_3)_2NNO_2$ and 2,2-dinitropropane $(CH_3)_2C(NO_2)_2$]. Lin et al.[17] reported a value of 43.7 kcal/mol for the activation energy for pyrolysis of $(CH_3)_2N-NO_2$, and this value can be compared with the activation energy of 45.7 kcal/mol we obtained for $(CH_3)_2C(NO_2)_2$. It appears that the $N-NO_2$ fission occurs somewhat more easily than bond breaking in $C-NO_2$. The much higher *A* factor for the pyrolysis of dimethylnitramine makes the $N-NO_2$ fission a faster process than $(O_2N)(>C)-NO_2$ bond fission. By extension one might conclude that $N-NO_2$ bond fission is more favorable than $C-NO_2$ fission in the pyrolysis of TNAZ over the temperature range 900−1200 K. However, it should be pointed out that the activation energies for the pyrolyses of both $(CH_3)_2N-NO_2$ and $(CH_3)_2C(NO_2)_2$ are several kilocalories higher than that of TNAZ (39.54 kcal/mol). Thus the bond strengths for both $C-NO_2$ and $N-NO_2$ may be reduced due to ring strain present in TNAZ.

The mechanism of the overall decomposition of 2,2-dinitropropane is complex. An extended mechanism of 90 elementary steps is presented in Table 1. To fully describe the pyrolysis over a wide range of temperature and pressure, we included in this mechanism numerous plausible steps. The rate constants for most of these reactions are available in the literature: the NIST Chemical Kinetics Database[25] is the principal source. For steps for which rate constants have not been reported, estimates were made based on values of analogous reactions as presented in the footnote to the table. Both the high and low pressure limit rate constants are listed in Table 1 for reactions in the falloff region, and the unimolecular rate constants for these steps were evaluated with the Lindemann expression. The rate equations from the mechanism were numerically integrated, and the calculated results were compared with the experimentally

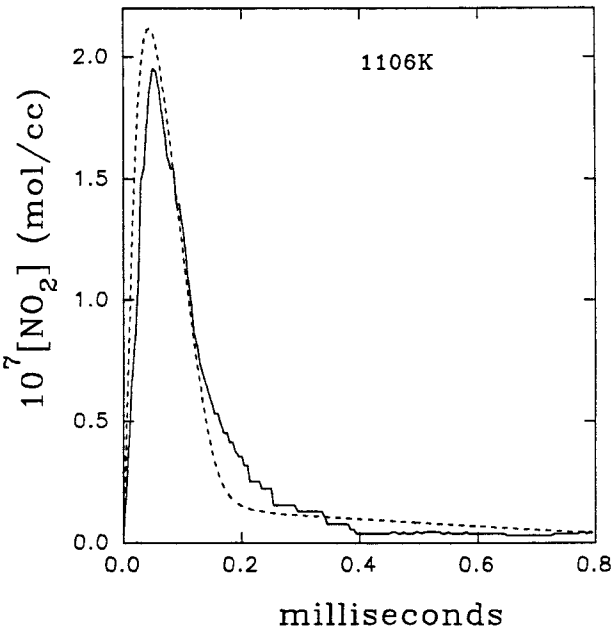

Figure 6. Solid line: Reduced experimentally recorded $[NO_2]$ vs time for 2,2-dinitropropane. Conditions: $T = 1106$, $P = 5.5$ atm, [2,2-dinitropropane]$_o = 5.1 \times 10^{-7}$ mol/cm^3. The dashed line is the computed $[NO_2]$ vs time curve, per the mechanism in Table 1.

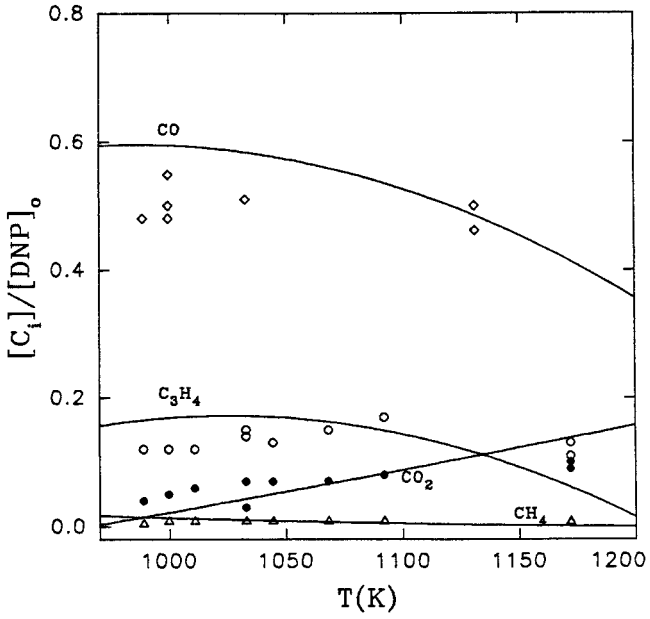

Figure 7. Observed vs computed product distributions developed during the thermal decomposition of 2,2-dinitropropane. The symbols are experimental values and the solid lines are based on numerical simulations per the mechanism in Table 1; residence time $\approx$ 1.5 ms.

derived values. The dashed lines in Figures 5 and 6 are the simulated NO_2 profiles; thus the agreement between the simulations and the experiments is very good. Figures 7−8 are the product distributions over the temperature range 970−1200 K, the symbols in the figures are experimental data and the lines are numerical simulations.

Per Table 1, pyrolysis is initiated by C−NO_2 fission from the *gem*-dinitro group, and the radicals NO_2 and $(CH_3)_2CNO_2$ are generated. $(CH_3)_2CNO_2$ then dissociates via three distinct pathways, as indicated in reactions 2, 3, and 10. $(CH_3)_2CNO_2$ may also react with NO_2 to produce $(CH_3)_2C(NO_2)(ONO)$, which rapidly dissociates to acetone, NO, and NO_2. This reaction was initially included in the mechanism, but it is not an

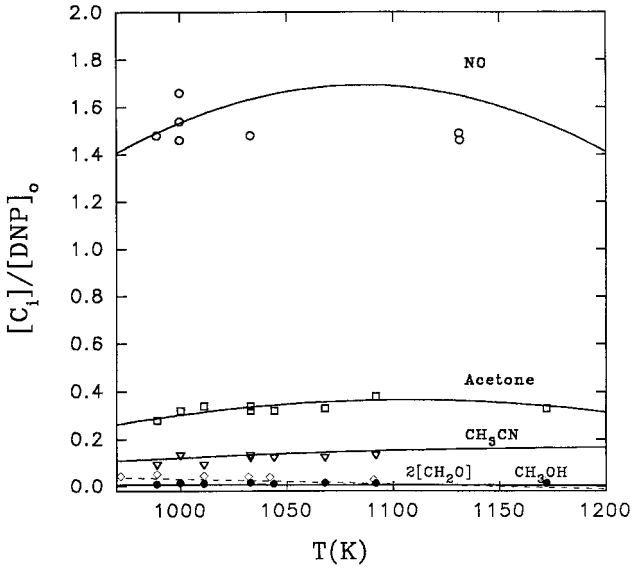

Figure 8. Observed vs computed product distributions developed during the thermal decomposition of 2,2-dinitropropane. The symbols are experimental values and the lines are based on numerical simulations, per the mechanism in Table 1. For clarity the open diamonds and the dashed line are two times the experimental and calculated values for CH_2O, respectively.

important step, since acetone is formed mainly by step 3. An important intermediate in the early part of the pyrolysis is $CH_2{=}C(CH_3)(NO_2)$ which rapidly dissociates through reactions 4, 5, and 6 to smaller fragments. As in the decomposition of most nitro compounds that we investigated, atomic H and OH radicals play critical roles. There are many steps in the mechanism, such as 2, 7, 8, 14, 21, and 55, that generate H atoms. The most important losses of H atoms are reactions with NO_2, $(CH_3)_2CNO_2$, NO, and DNP. The OH radical is generated mainly via the reaction between H and NO_2 (step 56) and by the dissociation of HONO (step 9). H reacts rapidly with $(CH_3)_2CO$, NO_2, H_2, CH_2O, and other species. Note that there are several secondary steps that consume 2,2-dinitropropane. However, these contributions to its overall decay are small (<10%). The calculated 2,2-dinitropropane vs time profiles with the proposed mechanism remain first order, but deviate slightly from those predicted by the measured unimolecular dissociation rate constant.

The initial build-up and the subsequent rapid consumption of NO_2, as shown in Figures 5 and 6, were also observed by Flournoy.[13] He attributed the rapid reduction of NO_2 to the reaction between NO_2 and acetone. A preliminary test of this reaction by Flournoy[13] indicated that it was fast at 100 °C. However, a detailed studied of this reaction by Jaffe[26] led to a rate constant that is too low to account for the loss of NO_2 in our shock-tube experiments. Since Flournoy's study was carried out in a closed vessel, over much lower temperature and pressure ranges, we undertook several preliminary tests of this reaction in the shock tube for the temperature range 1000−1200 K. We found that the reaction was indeed very slow, consistent with the rate constant reported by Jaffe. An analysis of the mechanism listed in Table 1 revealed that many reactions are responsible for the loss of NO_2. Beside those that are directly involved in the production and consumption of NO_2 such as 1, 4, 13, 56, 86, and 35, the rates of steps that involve H and OH are also important. For example, the reaction of OH with acetone generates CH_2COCH_3 that subsequently leads to the formation of H atom through reactions 43 and 44. Atomic H and OH

TABLE 1: 2,2-Dinitropropane Decomposition Mechanism[a]

no.[c]	reaction	A	n	E_a	ref
1	DNP → NO_2 + $(CH_3)_2CNO_2$	1.26E+13	0	45.7	*b*
2	$(CH_3)_2CNO_2$ → H + DNP(−HONO)	1.00E+11	0	30.0	*b,d*
3	$(CH_3)_2CNO_2$ → NO + $(CH_3)_2CO$	9.10E+12	0	40.0	*b,d*
4	DNP(−HONO) → NO_2 + CH_2═C(CH_3)	1.00E+14	0	35.0	*b*
5*	DNP(−HONO) → HONO + $CHCCH_3$	1.00E+11	0	37.0	*b,d*
6*	DNP(−HONO) → CH_2O + CH_3CNO	1.00E+11	0	37.0	*b,d*
7	CH_2═C(CH_3) → H + $CHCCH_3$	9.55E+12	0	46.11	27
8	CH_2═C(CH_3) → H + CH_2═C═CH_2	1.32E+13	0	47.69	27
9	HONO + (M) → OH + NO + (M)	1.09E+16	−1.23	49.69	28
		1.19E+21	−3.8	48.36	28
10	$(CH_3)_2CNO_2$ → CH_3O + CH_3CNO	1.21E+12	0	37.0	*b,d*
11	DNP + CH_3O → CH_3OH + DNP(−H)	3.00E+11	0	4.00	*b,d*
12	DNP + OH → H_2O + DNP(−H)	1.50E+12	0	0.00	*b*
13	DNP(−H) → NO_2 + DNP(−HONO)	1.00E+16	0	25.0	*b,d*
14	CH_3O + (M) → CH_2O + H+ (M)	3.16E+14	0	25.81	29
		4.82E+15	0	21.51	29
15*	CH_3O + NO → CH_2O + HNO	2.41E+12	−0.7	0	30
16	CH_3O + NO → CH_3ONO	1.21E+13	0	0	31
17	CH_3ONO → CH_3O + NO	6.31E+15	0	41.20	32
18*	CH_3ONO → HNO + CH_2O	3.98E+13	0	38.50	32
19	CH_2O + M → H_2 + CO+ M	2.10E+15	0	35.01	33
20	CH_2O + H → H_2 + HCO	5.25E+12	1.77	3.00	34
21	HCO + M → H + CO + M	2.59E+12	−2.14	20.42	35
22	HCO + NO → HNO + CO	7.23E+12	0	0	28
23*	CH_3O + CH_2O → CH_3OH + HCO	1.02E+11	0	2.981	35
24*	CH_3O +OH → CH_2O + H_2O	1.81E+13	0	0.00	35
25	CH_3O + HNO → CH_3OH + NO	3.16E+13	0	0.00	36
26*	CH_3O + HCO → CH_3OH + CO	9.04E+13	0	0.00	35
27*	CH_3O +NO_2 → CH_2O + HONO	5.01E+11	0	0.00	32
28*	H + H + M → H_2 + M	2.19E+15	−1.0	0.00	37
29*	H + OH + M → H_2O + M	2.49E+17	−2.0	0.00	37
30**	HNO + HNO → H_2O + N_2O	8.43E+08	0	3.10	28
31	HNO → H + NO	1.04E+15	−0.43	49.53	28
32	H + NO → HNO	1.47E+14	−0.41	0.00	28
33	HNO + CH_3 → CH_4 + NO	2.00E+12	0	0.00	38
34	HNO + OH → H_2O + NO	4.82E+13	0	0.994	28
35	HNO + NO_2 → HONO + NO	1.00E+13	0	0.00	28
36*	HNO + HCO → NO + CH_2O	6.03E+11	0	1.987	28
37	CH_3CNO + NO → CH_3CN + NO_2	1.00E+13	0	0.00	*b,d*
38	CH_3CNO + H → CH_3CNOH	1.00E+14	0	0.00	*b,d*
39	CH_3CNOH → CH_3CN + OH	1.00E+16	0	35.0	*b,d*
40*	$(CH_3)_2CO$ + NO_2 → HONO + CH_2COCH_3	3.80E+05	0	7.13	26
41	$(CH_3)_2CO$ + OH → H_2O + CH_2COCH_3	1.51E+11	0	0	39
42	CH_2COCH_3 → CH_2CO + CH_3	1.00E+16	0	30.0	*b,d*
43	CH_2CO + OH → CH_2OH + CO	1.02E+13	0	0	37
44	CH_2OH + (M) → CH_2O + H + (M)	7.00E+14	0	29.63	29
		1.21E+16	0	25.81	29
45*	CH_2OH + H_2O → CH_3OH + OH	1.55E+14	0	26.29	40
46*	CH_2OH + H_2 → CH_3OH + H	6.00E+10	2	13.36	41
47*	CH_2OH + OH → CH_2O + H_2O	2.41E+13	0	0	41
48*	CH_2OH + H → CH_3 + OH	9.64E+13	0	0	41
49*	CH_2OH + H → CH_2O + H_2	6.03E+12	0	0	41
50*	CH_2OH + HCO → CH_3OH + CO	1.21E+14	0	0	41
51*	CH_2OH + HCO → CH_2O + CH_2O	1.81E+14	0	0	41
52	$(CH_3)_2CO$+ CH_3 → CH_4 + CH_2COCH_3	4.50E+11	0	10.53	42
53	OH + NO_2 → $HONO_2$	3.61E+13	0	0	43
54	$HONO_2$ + (M) → OH + NO_2 + (M)	3.99E+13	0	47.7	44
		2.20E+17	0	40.0	44
55	OH + H_2 → H + H_2O	2.74E+14	0	7.70	45
56	H + NO_2 → OH + NO	4.00E+13	0	0	46
57	CH_3 + OH → CH_3OH	1.15E+20	−8.2	11.67	47
58	CH_3 + CH_3O → CH_2O + CH_4	2.41E+13	0	0	35
59	CO + OH → CO_2+ H	3.25E+10	1.5	−0.497	37
60*	HCO + NO_2 → CO + HONO	8.97E+14	−3.29	2.36	48
61*	CO + NO_2 → CO_2 + NO	9.04E+13	0	33.78	49
62	CH_3 + NO_2 + (M) → CH_3NO_2 + (M)	2.07E+13	−0.6	0	50
		3.59E+20	−6	0	50
63	CH_3NO_2 + (M) → CH_3 + NO_2 + (M)	1.78E+16	0	58.5	51
		1.26E+17	0	42.0	51
64	CH_3 + NO_2 → CH_3O + NO	1.30E+13	0	0	50
65	CH_3 + NO_2 → CH_2O + HNO	3.22E+12	0	0	52
66	H + DNP → DNP(−H) + H_2	1.50E+13	0	0	*b,d*
67	H + DNP → HONO + $(CH_3)_2CNO_2$	5.00E+12	0	0	*b,d*
68	CH_3O + NO_2 → CH_3ONO_2	7.94E+12	0	0	53

TABLE 1 (Continued)

no.[c]	reaction	A	n	E_a	ref
69	$CH_3ONO_2 \rightarrow CH_3O + NO_2$	1.00E+13	0	33.39	54
70*	$CH_3ONO_2 + OH \rightarrow CH_3O + HONO_2$	1.81E+11	0	0	55
71*	$CH_2O + NO_2 \rightarrow HONO + HCO$	1.26E+13	0	26.70	56
72**	$CH_2COCH_3 + NO_2 \rightarrow ONOCH_2COCH_3$	5.00E+13	0	0	*b,d*
73**	$ONOCH_2COCH_3 \rightarrow CH_2ONO + CH_3CO$	1.00E+13	0	25.16	*b,d*
74**	$CH_2ONO \rightarrow CH_2O + NO$	1.00E+15	0	35.23	*b,d*
75**	$CH_3CO + (M) \rightarrow CH_3 + CO + (M)$	2.80E+13	0	17.15	57
		6.03E+15	0	14.07	57
76	$CH_2{=}C(CH_3){+}OH \rightarrow (CH_3)_2CO$	4.00E+12	0	0	*b,d*
77*	$H + HCO + M \rightarrow CH_2O + M$	1.16E+18	−2.57	0.427	58
78*	$H_2 + NO_2 \rightarrow H + HONO$	2.41E+13	0	28.82	28
79	$OH + CH_2O \rightarrow H_2O + HCO$	3.00E+13	0	1.194	59
80*	$H + CO_2 \rightarrow CO + OH$	1.00E+11	0	0	*b,d*
81	$OH + CHCCH_3 \rightarrow H_2O + CHCCH_2$	1.50E+12	0	0	60
82	$OH + CH_2{=}C{=}CH_2 \rightarrow H_2O + CHCCH_2$	1.50E+12	0	0	60
83	$NO + CHCCH_2 \rightarrow CHCCH_2NO$	1.00E+13	0	0	*b,d*
84	$NO_2 + NO_2 \rightarrow NO + NO + O_2$	2.00E+12	0	25.1	61
85**	$NO_2 + CH_2COCH_3 \rightarrow CH_3CO + NO + CH_2O$	1.00E+14	0	0	*b,d*
86	$CH_2{=}C(CH_3) + NO_2 \rightarrow CH_2COCH_3 + NO$	4.00E+10	0	0	*b,d*
87	$NO_2 + CH_2COCH_3 \rightarrow OCH_2COCH_3 + NO$	1.00E+13	0	0	62
88	$OCH_2COCH_3 \rightarrow CH_3CO + CH_2O$	1.00E+14	0	0	*b,d*
89	$H + (CH_3)_2CNO_2 \rightarrow H_2 + DNP(-HONO)$	7.50E+13	0	0	*b,d*
90*	$H + CH_3ONO \rightarrow CH_3OH + NO$	1.22E+11	0	1.9	63

[a] Abbreviations and symbols in the table: DNP −− 2,2-dinitropropane; DNP(−HONO) −− $CH_2{=}C(CH_3)(NO_2)$; DNP(−H) −− $\bullet CH_2{-}C(CH_3)_2(NO_2)$. [b] Values assigned in this report. [c] Reactions marked with asterisks are "unimportant" under the experimental conditions in this report, and those marked with double asterisks can also be eliminated from the mechanism if only the important species need to be reproduced. [d] The values for the following rate constants, in Table 1, were estimated. Reaction 2 is analogous to the dissociation of C_2H_5 to C_2H_4 and H, for which the reported unimolecular rate constant is $2.9 \times 10^{11}\exp\{(-33.8\ \text{kcal/mol})/RT\}\ s^{-1}$. A similar value, $10^{11}\exp\{(-30\ \text{kcal/mol})/RT\}\ s^{-1}$ was chosen to best fit our data. Reaction 3 was proposed several times previously, but its rate constant was not measured. It appears to pass through the $NO_2 \rightarrow$ ONO isomerization, and then dissociates to yield $(CH_3)_2CO$ and NO. This isomerization step typically has a relatively tight transition state and the activation energy is in the range 30−45 kcal/mol. $9.1 \times 10^{12}\ \exp\{(-40\ \text{kcal/mol})/RT\}$ was chosen for 3 to best fit our data. Reaction 5, 6, and 10 are multiple center elimination reactions. Their rate constants were chosen from the published data for the HONO elimination in mononitro compounds. Reaction 11 is analogous to $CH_3O + CH_4 \rightarrow CH_3OH + CH_3$, for which the rate constant over the temperature range 300−2500 K is $1.57 \times 10^{11}\exp\{(-8.8\ \text{kcal/mol})/RT\}$. A rate constant, with similar magnitudes for the Arrhenius parameters was chosen for reaction 11. The rate constant for H abstraction from HNO_2 by OH is $\sim 1.5 \times 10^{12}$ with little activation energy. This value was used for reaction 12 to best fit our experimental data. Reaction 13 is a typical $C{-}NO_2$ bond fission with a loose transition state, but the activation energy is expected to be much lower than for the corresponding stable compound. The rate constant in Table 1 is an estimated value that best fits our experimental data. Reactions 37, 38, and 39 have been proposed previously to rationalize the formation of CH_3CN in similar systems. The rate constant for reaction 37 was derived from the analogous reaction $CF_3OO + NO \rightarrow NO_2 + CF_3O$ for which the rate constant is 1.06×10^{13} cm^3/(mol-s). The rate constant for reaction 38 was deduced from the analogous reaction between CH_3O and H; and the rate constant for reaction 39 was chosen to fit the CH_3CN data. The A factor for reaction 42 was derived from similar bond fission reactions, its activation energy was chosen to fit the data. Typical Arrehnius parameters for the abstraction reaction H + hydrocarbon $\rightarrow H_2$ + radical are: $10^{13}-10^{14}$ for the *A* factor, with a very low activation energy. The value 1.5×10^{13} was chosen for reaction 66. The rate constant for reaction 67 was estimated from the rate constant for the reaction between H and CH_3NO_2. The reported value for reaction 72 at 298 K is 1×10^{13}. We chose 5×10^{13}, and for reaction 73:$1 \times 10^{13}\ \exp\{(-25.16\ \text{kcal/mol})/RT\}$, for the temperature range 800−1100 K to best fit our data. The rate constant for reaction 74 was assumed to be similar to that for the reaction $CH_3ONO \rightarrow CH_3O + NO$. Rate constants for reactions 76, 80, 85, 86, and 89 were chosen to fit our data. The rate constant for reaction 83 was deduced from the reported value for the analogous reaction $CH_3 + NO \rightarrow CH_3NO + CH_2O$. The rate constant for reaction 88 was derived from the reaction $CH_3CH_2O \rightarrow CH_3 + CH_2O$.

radicals produced in later reactions are partly responsible for the rapid falloff of the NO_2 after its initial build-up.

The reaction between OH and NO_2 leads to the formation of HNO_3, which was observed in our product mixture. The concentration of this compound in the predicted product mixture is low (∼2% of initial 2,2-dinitropropane concentration), and it decreases with rising temperature. The model also predicts the formation of some $CH{\equiv}C{-}CH_2NO$ and $CH_2{=}C{=}CHNO$ from the reactions of NO with $CHCCH_2$. The existence of these compounds in the product samples was not established with our analytical techniques.

NO_2 is transient in the pyrolyses of both 2-nitropropane and 2,2-dinitropropane. However, their NO_2 profiles are quite different. The peak values of NO_2 that are generated in the dinitro species are more than two times higher than those for the mono compound, and its initial build-up and subsequent decay are also much faster. This is partly due to the fact that the unimolecular dissociation rate constant of the dinitro compound is ∼1.5 times larger, but mainly due to the differences in the fragmentation patterns of the two compounds. In the case of DNP, larger levels of H and OH, formed during the later stages of the reaction, lead to a somewhat delayed but more rapid decay of NO_2.

Sensitivity Analysis

The mechanism in Table 1 was subjected to the sensitivity/principal component analysis we described previously.[8] The following criteria were used to determine the importance of each step in the mechanism: a step is considered *important* if it belongs to a reaction group with an eigenvalue $\geq 1.0 \times 10^{-5}$, and is considered *unimportant* for a lower eigenvalue. However, if the eigenvector of a reaction is less than 0.1, it is also considered unimportant, regardless of the magnitude of the corresponding eigenvalue. The mechanism in Table 1 was first analyzed assuming that all 43 species in the mechanism are "observed", under the stipulation that the reduced mechanism reproduces the profiles of all these species to within ∼5%. The results of this analysis indicated that there are 27 steps in the mechanism that are not important during any part of the

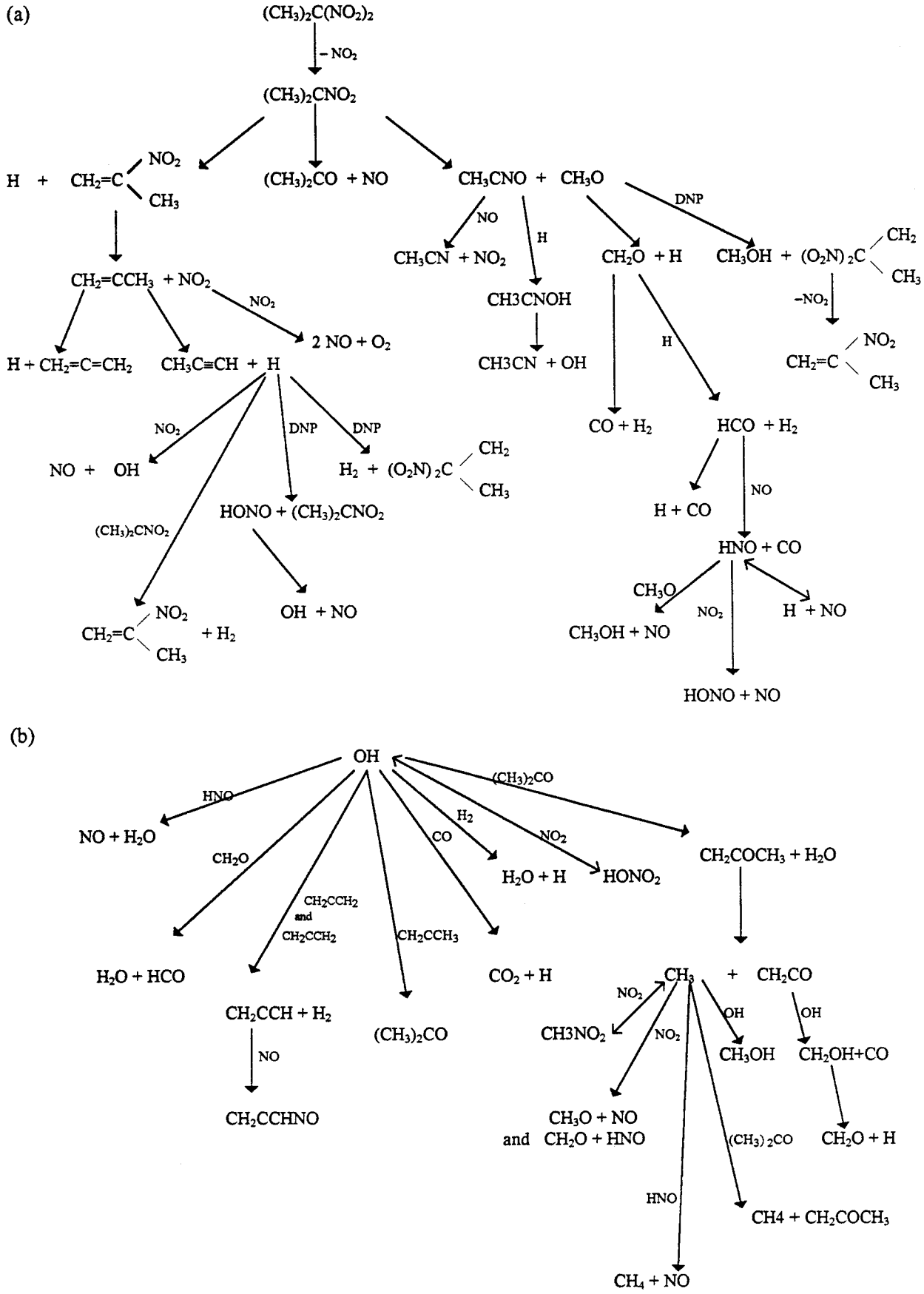

Figure 9. Fragmentation and reaction sequence in the thermal decomposition of 2,2-dinitropropane.

conversion. These are marked with a single asterisk in Table 1. The mechanism can be further reduced by considering only those species as "observed" for which the concentration during the conversion is relatively high ($> 10^{-4}$[2,2-dinitropropane]$_o$). Six more reactions were identified as redundant. These steps are marked with double asterisks in Table 1. Results from numerical

simulations with the reduced mechanism indicated that indeed the temporal profiles of the "observed" species agree with those generated from the full mechanism to within 5%. The fragmentation and reaction sequence based on the simplified mechanism is presented graphically in Figure 9. Note the critical roles of H, OH, NO_2, HNO, HCO, and $(CH_3)_2CNO_2$ in the overall conversion. It should be noted that although the simulations based on the proposed mechanism reproduce the experimentally analytical values very well, some uncertainties remain. The rate constants for a number of important steps in the mechanism need to be confirmed experimentally. However, we believe that the principal features of the pyrolysis of 2,2-dinitropropane over the temperature range 970−1200 K have been presented.

Acknowledgment. This work was supported by the Army Research Office under Grant NO. DAAH04-95-1-0130. We thank Professor Peter Jeffers of SUNY at Cortland for help with the identification of some of the pyrolysis products through GC/MS.

References and Notes

(1) Urbanski, T. *Chemistry and Technology of Explosives*; Pergamon Press: New York, 1964.
(2) Albright, R. E.; Nelson, F. L.; Raymond, L. *Ind. Eng. Chem*. **1949**, *41*, 929.
(3) Anex, D. S.; Allman, J. C.; Lee, Y. T. In *Chemistry of Energetic Materials*; Olah, G. A., Squire, D. R., Eds.; Academic Press: New York, 1991; Chapter 2.
(4) Zhang, Y.-X.; Bauer, S. H. *J. Phys. Chem. A* **1998**, *102*, 5846.
(5) Oyumi, Y.; Brill, T. B. *Combust. Flame* **1985**, *62*, 225.
(6) Oxley, J.; Smith, J.; Zheng, W.; Roger, E.; Coburn, M. *J. Phys. Chem. A* **1997**, 101, 4375.
(7) Garland, N. L.; Nelson, H. H. *J. Phys. Chem. B* **1998**, *102*, 2663.
(8) Zhang, Y.-X.; Bauer, S. H. *J. Phys. Chem. B* **1997**, *101*, 8717.
(9) Zhang, Y.-X.; Yu, C-. L.; Bauer, S. H. *Int. J. Chem. Kinet*. **1998**, *30*, 185.
(10) Zhang, Y.-X.; Bauer, S. H. *J. Phys. Chem*. *104*, 1207.
(11) Wilcox, C. F.; Zhang, Y.-X.; Bauer, S. H. *J. Mol. Struct. (THEOCHEM)*, in press.
(12) Garver, L. C.; Grakauskas, V.; Baum, K. *J. Org. Chem*. **1985**, *50*, 1699.
(13) Flournoy, J. M. *J. Chem. Phys*. **1962**, *36*, 1107.
(14) Buczkowski, Z.; Urbanski, T. *Spectrochim. Acta* **1966**, *22*, 227.
(15) Shishkov, I. F.; Sadova, N. I.; Vilkov, L. V.; Pankrushev, Yu. A. *Zh. Strukt. Khim*. **1983**, *24*, 173.
(16) Flournoy, J. M. *J. Chem. Phys.* **1962**, *36*, 1106.
(17) Lloyd, S. A.; Umstead, M. E.; Lin, M. C. *J. Energ. Mat*. **1985**, *3*, 187.
(18) Shaw, R. *Int. J. Chem. Kinet*. **1973**, *5*, 261.
(19) Leroy, G.; Sana, M.; Wilante, C.; Peeters, D.; Bourasseau, S. *J. Mol. Struct. (THEOCHEM*) **1989**, *56*, 251.
(20) Wodkte, A. M.; Hintsa, E. J.; Lee, Y. T. *J. Phys. Chem*. **1986**, *90*, 3549.
(21) Wilde, K. *Ind. Eng. Chem*. **1956**, *48*, 769.
(22) Smith, T. E.; Calvert, J. G. *J. Phys. Chem*. **1959**, *63*, 1305.
(23) Politzer, P.; Lane, P.; Grice, M. E.; Concha, M. C.; Redfern, P. C. *J. Mol. Struct. (THEOCHEM)* **1995**, *338*, 249.
(24) Politzer, P.; Seminario, J. M. *Chem. Phys. Lett*. **1993**, *207*, 27.
(25) Mallard, W. G.; Westley, F.; Herron, J. T.; Hampson, R. F.; Frizzel, D. H. *NIST Chemical Kinetics Database*; U.S. Department of Commerce, 1998.
(26) Jaffe, S. *Chem. React. Urban Atmos. Proc. Symp*. **1971**, *1969*, 103.
(27) Naroznik, M.; Niedzielski, J. *J. Photochem*. **1986**, *32*, 281.
(28) Tsang, W.; Herron, J. T. *J. Phys. Chem. Ref. Data* **1991**, *20*, 609.
(29) Greenhill, P. G.; O'Grady, B. V.; Gilbert, R. G. *Aust. J. Chem*. **1986**, *39*, 1929.
(30) Atkinson, R.; Baulch, D. L.; Cox, R. A.; Hampson, R. F., Jr.; Kerr, J. A.; Rossi, M. J.; Troe, J. *J. Phys. Chem. Ref. Data* **1997**, *26*, 521−1011.
(31) Batt, L.; Milne, R. T. *Int. J. Chem. Kinet.* **1974**, *6*, 945.
(32) Batt, L.; Milne, R. T.; McCulloch, R. D. *Int. J. Chem. Kinet*. **1977**, *9*, 567.
(33) Miyauchi, T.; Mori, Y.; Imamura, A. *Symp. Int. Combust. Proc*. **1977**, *16*, 1073.
(34) Hidaka, Y.; Taniguchi, T.; Tanaka, H.; Kamesawa, T.; Inami, K.; Kawano, H. *Combust. Flame* **1993**, *92*, 365−376.
(35) Tsang, W.; Hampson, R. F. *J. Phys. Chem. Ref. Data* **1986**, *15*, 1087.
(36) He, Y.; Sanders, W. A.; Lin, M. C. *J. Phys. Chem*. **1988**, *92*, 5474.
(37) Baulch, D. L.; Cobos, C. J.; Cox, R. A.; Esser, C.; Frank, P.; Just, Th.; Kerr, J. A.; Pilling, M. J.; Troe, J.; Walker, R. W.; Warnatz, J. *J. Phys. Chem. Ref. Data* **1992**, *21*, 411−429.
(38) Laidler, K. J.; Sagert, N. H.; Wojciechowski, B. W. *Proc. R. Soc. London* **1962**, *270*, 254−266.
(39) Kerr, J. A.; Stocker, D. W. *J. Atmos. Chem*. **1986**, *4*, 253.
(40) Tsuboi, T.; Hashimoto, K. *Combust. Flame* **1981**, *42*, 61.
(41) Tsang, W. *J. Phys. Chem. Ref. Data* **1987**, *16*, 471.
(42) Kinsman, A. C.; Roscoe, J. M. *Int. J. Chem. Kinet*. **1994**, *26*, 191−200.
(43) Wine, P. H.; Kreutter, N. M.; Ravishankara, A. R. *J. Phys. Chem.* **1979**, *83*, 3191.
(44) Glaenzer, K.; Troe, J. *Ber. Bunsen-Ges. Phys. Chem*. **1974**, *78*, 71.
(45) Leroy, G.; Sana, M.; Tinant, A. *Can. J. Chem*. **1985**, *63*, 1447−1456.
(46) Agrawalla, B. S.; Manocha, A. S.; Setser, D. W. *J. Phys. Chem*. **1981**, *85*, 2873.
(47) Dean, A. M.; Westmoreland, P. R. *Int. J. Chem. Kinet*. **1987**, *19*, 207.
(48) Lin, C.-Y.; Wang, H.-T.; Lin, M. C.; Melius, C. F. *Int. J. Chem. Kinet*. **1990**, *22*, 455−482.
(49) Tsang, W.; Herron, J. T. *J. Phys. Chem. Ref. Data* **1991**, *20*, 609−663.
(50) Glaenzer, K.; Troe, J. *Ber. Bunsen-Ges. Phys. Chem*. **1974**, *78*, 182.
(51) Glaenzer, K.; Troe, J. *Helv. Chim. Acta* **1972**, *55*, 2884.
(52) Canosa, C.; Penzhorn, R.-D.; von Sonntag, C. *Ber. Bunsen-Ges. Phys. Chem*. **1979**, *83*, 217.
(53) Batt, L.; Rattray, G. N. *Int. J. Chem. Kinet*. **1979**, *11*, 1183.
(54) Zaslonko, I. S.; Smirnov, V. N.; Tereza, A. M. *Kinet. Catal*. **1993**, *34*, 531−538.
(55) Nielsen, O. J.; Sidebottom, H. W.; Donlon, M.; Treacy, *J. Chem. Phys. Lett*. **1991**, *178*, 163.
(56) Fifer, R. A. *Ber. Bunsen-Ges. Phys. Chem*. **1975**, *10*, 613.
(57) Baulch, D. L.; Cobos, C. J.; Cox, R. A.; Frank, P.; Hayman, G.; Just, Th.; Kerr, J. A.; Murrells, T.; Pilling, M. J.; Troe, J.; Walker, R. W.; Warnatz, J. *J. Phys. Chem. Ref. Data* **1994**, *23*, 847.
(58) Eiteneer, B.; Yu, C.-L.; Goldenberg, M.; Frenklach, M. *J. Phys. Chem. A* **1998**, *102*, 5196.
(59) Warnatz, J. In *Combustion Chemistry*; Gardiner W. C., Jr., Ed.; Springer-Verlag: New York, 1984.
(60) Atkinson, R.; Aschmann, S. M. *Int. J. Chem. Kinet*. **1984**, *16*, 259.
(61) Rohrig, M.; Petersen, E. L.; Davidson, D. F.; Hanson, R. K. *Int. J. Chem. Kinet*. **1997**, *29*, 483.
(62) Sehested, J.; Christensen, L. K.; Nielsen, O. J.; Bilde, M.; Wallington, T. J.; Schneider, W. F.; Orlando, J. J.; Tyndall, G. S. *Int. J. Chem. Kinet*. **1998**, *30*, 475−489.
(63) Moortgat, G. K.; Slemr, F.; Warneck, P. *Int. J. Chem. Kinet*. **1977**, *9*, 249.